



HAL
open science

Modelling of migration and orientation of endothelial cells on micropatterned polymers

Julie Joie, Y. Lei, Thierry Colin, Marie-Christine Durrieu, Clair Poignard,
Olivier Saut

► **To cite this version:**

Julie Joie, Y. Lei, Thierry Colin, Marie-Christine Durrieu, Clair Poignard, et al.. Modelling of migration and orientation of endothelial cells on micropatterned polymers. [Research Report] RR-8252, INRIA. 2013. hal-00795238v2

HAL Id: hal-00795238

<https://inria.hal.science/hal-00795238v2>

Submitted on 14 May 2014

HAL is a multi-disciplinary open access archive for the deposit and dissemination of scientific research documents, whether they are published or not. The documents may come from teaching and research institutions in France or abroad, or from public or private research centers.

L'archive ouverte pluridisciplinaire **HAL**, est destinée au dépôt et à la diffusion de documents scientifiques de niveau recherche, publiés ou non, émanant des établissements d'enseignement et de recherche français ou étrangers, des laboratoires publics ou privés.



Modelling of migration and orientation of endothelial cells on micropatterned polymers

J. Joie, Y. Lei, T. Colin, M.-C. Durrieu, C. Pognard, O. Saut

**RESEARCH
REPORT**

N° 8252

February 2013

Project-Teams MC2



Modelling of migration and orientation of endothelial cells on micropatterned polymers

J. Joie, Y. Lei, T. Colin, M.-C. Durrieu, C. Pognard*, O. Saut

Project-Teams MC2

Research Report n° 8252 — February 2013 — 19 pages

Abstract: Understanding the cell migration on micropatterned polymers, as well as their orientation is a critical issue in tissue engineering, since it is the preliminary step in the blood vessel formation. In this paper, we derive an agent-based model to describe the migration and the orientation of endothelial cells seeded on bioactive micropatterned polymers. The model is obtained thanks to the experimental observations, and it provides numerical results that are quantitatively in accordance with the experimental data.

Key-words: Tissue engineering; biomathematical modeling; agent-based model; endothelial cells; migration; differential equations

* Corresponding author: clair.pognard@inria.fr

**RESEARCH CENTRE
BORDEAUX – SUD-OUEST**

351, Cours de la Libération
Bâtiment A 29
33405 Talence Cedex

Modélisation de la migration et de l'orientation de cellules endothéliales

Résumé : La compréhension de la migration et de l'orientation de cellules contrôlées géométriquement est un point crucial dans le contexte de l'ingénierie tissulaire. Il s'agit en effet de la première étape pour la formation de vaisseaux sanguins. Dans cet article, nous avons établi un modèle d'agent décrivant la migration et l'orientation de cellules endothéliales dispersées sur des plaques composées de polymères bioactifs. Ce modèle est basé sur des considérations expérimentales et nous avons pu obtenir des résultats quantitativement en accord avec ces expériences.

Mots-clés : Ingénierie tissulaire ; modélisation bio-mathématique ; modèles d'agents, cellules endothéliales ; migration ; équation différentielles

Contents

1	Introduction	4
2	Experimental studies	5
3	Description of the model	7
3.1	Net force acting on the cell	7
3.1.1	Cell-to-cell attraction force \mathbf{F}_c	8
3.1.2	Repulsive force	9
3.1.3	Friction force	10
3.1.4	Attractive force of the adhesive areas	10
3.2	Orientation of the cells	10
3.2.1	Heuristics of cell alignment	10
3.2.2	Differential equation for \mathbf{L}_i	11
4	Simulations and experiments	11
4.1	Numerical method	12
4.2	Calibration of the model	12
4.2.1	Cell shape	12
4.3	Qualitative results on the cell motility towards the micropatterns	13
4.4	Quantitative results on cell alignment	13
4.5	Sensitivity analysis	15
5	Conclusion	16

1 Introduction

Tissue engineering is the use of combination of cells, engineering, materials, and suitable biochemical factors to improve or replace biological functions [21]. A major problem for the creation of tissue *in vitro* is the lack of functional microvasculature networks. Indeed, the role of capillaries and blood vessels is to supply oxygen and nutrients to the cells, but also to remove waste products and CO₂ [12]. Without an efficient vessel network, the size of cultured tissues is limited by the weak diffusion of nutrients. The understanding of the mechanisms involved in the creation of new blood vessel is therefore crucial.

One strategy to develop clinical implants consists of appropriate utilizations of bioactive materials: bioactive materials may induce *in vivo* regenerative response at the site of damage, whereas when used *in vitro*, they can stimulate the tissue growth for subsequent implantation [1], [16]. Different bioactive ligands have been used to study their effects on cell functions for a better understanding of vascularization [23]. In the aim of promoting angiogenesis in the case of tissue engineering or of inhibiting angiogenesis in the case of cancer, it is important to understand the mechanisms that regulate lumen formation. Successful micropatterning of cells is becoming a key component of this field [11].

Researchers are currently interested in the behavior of cells on substrates that have been patterned by micro- or nano-fabrication [8, 22]. As reported by Chen *et al.* in [3], cell positioning and physiology can be controlled by the substrate on which the cells adhere. Experiments presented by Lei *et al.* in [15, 16] show that the use of cell adhesion peptides that are micropatterned onto material makes possible the formation of tube-like structures unlike the use of homogeneously grafted materials.

More precisely, experimental studies using micropatterned substrates revealed that the cell migration is governed by the geometry of patterns. So cultured endothelial cells form extensive cell-cell interactions, and in some configurations, the accumulation of endothelial cell junctions implies that tube-like structures are created. The goal of the present paper is to provide a simple model that describes quantitatively the cell migration towards the micropatterns and the final orientation of the cells on the strips.

In a previous work [4], we have derived a continuous model of cell migration based on the well-known Patlak-Keller-Segel model for chemotaxy. That approach made possible qualitative description of the evolution of endothelial cell densities in accordance with the experiments. In particular we have shown the high influence of the geometry and of the initial cell density on the migration.

Nevertheless such a continuous model does not take the cell orientation into account, which is an important experimental data since it describes the cell organization on the micropatterns. Cell orientation on the micropatterns plays a crucial role in the formation of tube-like structures, and the aim of this work is to propose a simple model that can account for it.

Since the experiments deal with a quit small number of cells (around 50 000 per cm²), unlike [4], it is relevant to consider each cell separately and we describe cell-to-cell interactions for a large number of cells. We refer to [6, 24] for agent-based models that describe cell-cel interactions. We emphasize that the idea is to propose a very simple model that can be fitted to produce quantitative results in accordance with the data. We thus started from the biological observations of the phenomena, and we derive our models thanks to simple mechanics considerations.

Polarization of cells can be an active phenomena induced by external causes (see [9],[18], [2]). Nevertheless in some cases polarization can be observed without any external stimulations as reported in [10], [26] and [25]. Therefore, we have chosen some *ad hoc* rules of cell alignment in order to model the cell orientation. These phenomenological and simple rules account for the complex phenomenon of cell orientation, which is probably a mixing of the effect of the micro

patterned and of non observable phenomena.

The outline of this article is the following: in the first part we present the experimental techniques and the data that are available. We then describe the set of equations defining the model, before presenting numerical results. We also show the consistency of our model, by comparing quantitatively both numerical and experimental data. It is very striking and interesting that our very simple model, which is only based on classical mechanics without any description of the complex molecular interactions, provides results that are quantitatively in accordance with the experiments.

2 Experimental studies

The experimental results have been precisely presented in [15, 16]. We only remind the reader of the main observations given in these papers. The micropatterned polymers are adhesive areas composed of cell adhesion peptides or growth factors peptides that make the cells adhere. These areas are surrounded by non-adhesive areas on which cells move freely [15]. Human umbilical vein endothelial cells (HUVECs) were isolated from the human umbilical cord vein. HUVECs were grown on gelatin coated culture flasks in a complete HUVEC culture medium. HUVECs are seeded onto micropatterned bioactive materials during several hours, then they are washed out. Only the adhered endothelial cells remain on material. The initial cell density is around 50 000 cells per cm^2 (see [15]).

Active principles (cell adhesion peptides or growth factors) do not diffuse in the domain. Therefore endothelial cells outside adhesive areas have no means to "feel" directly these areas. They find out these areas indirectly, by the chemoattractant produced by the cell that are already on the strip. Actually, during the migration phase, we observe that cells have a random motility and stop on adhesive areas. Moreover the attraction of endothelial cells on adhesive areas seems to be higher than the one of cells outside those areas. Note that throughout the paper we do not consider the influence of nutrients and we assume that cells obtain enough nutrients from the material (due to grafted active principles onto material).

In Fig.1, the final position of the cells on two different micropatterns are observed. Fig.1(a) shows the case of thin adhesive areas of $10\ \mu\text{m}$ width with an inter-pattern separation of $100\ \mu\text{m}$, whereas Fig.1(b) shows the end of the migration on large strips (bioactive pattern size: $300\ \mu\text{m}$ and distance between patterns: $100\ \mu\text{m}$). For a detailed description of such experiments, one may refer to [15].

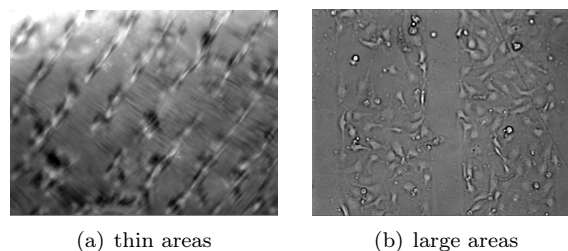


Figure 1: Endothelial cells alignment onto micropatterned polymer (PET) ($10\ \mu\text{m}$ (a) and $300\ \mu\text{m}$ (b) stripes of cell adhesion peptides) [15]. The distance between bioactive patterns is $100\ \mu\text{m}$.

It has been observed that cells tend to gather along the micropatterns. Note that the cells located on the adhesive areas still move along the strip: they are not completely stuck on

the adhesive area, but they do not leave the strips. Note also that according to pattern size, endothelial cells line their cytoskeleton to adjust it with the adhesive area.

As presented in [15], the orientation of the endothelial cells is strongly influenced by the width of the patterns. Fig. 2 shows cells on different widths of strips . One can also notice that, on

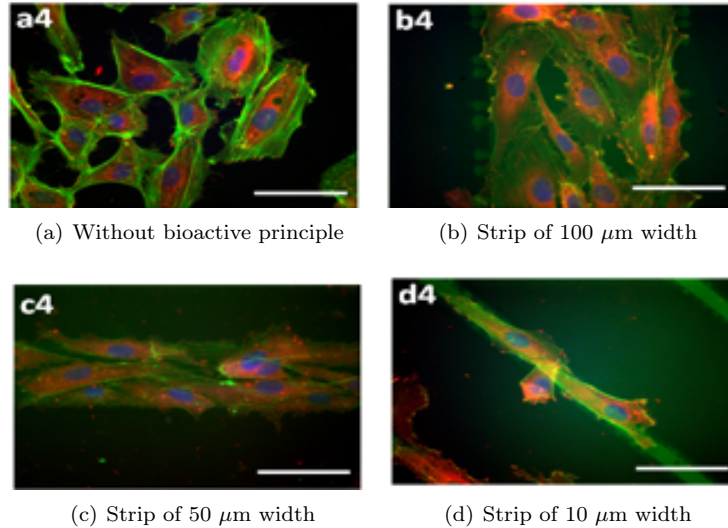


Figure 2: Endothelial cells alignment on different micropatterned polymers (PET) (strips of RGDS peptides), [15]

micropatterns of 10 μm thin strips, tubes containing a central lumen may appear [15],[5]. In other words, blood vessels are created from an initial random density of endothelial cells. Such phenomenon is not observed with larger strips [5],[13],[17].

Our goal is to predict quantitative information on the influence of the micropatterned geometry on both cell migration and alignment. The following facts have been observed experimentally:

- Initially, cells have a random motility and stop on the adhesive areas.
- The attractive force between cells is important.
- Cells on adhesive areas more strongly pull their neighbors and still have a very low motility.
- Two cells cannot stack themselves.
- If part of a cell body is located on a strip, it tries to completely enter the strip.
- Cells tend to align themselves with their neighbors.

We aim at deriving a model that describes precisely these phenomena. Note that since the cell deformation during the migration is a very complex process, which is still poorly understood, we choose to consider a simple cell shape, namely in the paper, the cells are ellipses whose parameters depend on the configuration of the experiments.

3 Description of the model

Since the experimental data deal with a quite small number of cells, the continuous model derived in [4] cannot provide results that could be quantitatively compared to the experiments. The use of a discrete model has been preferred here to describe the cell migration on the micropatterns at the microscopic level. We therefore aim at deriving a model that describes both motility and orientation of a single cell, with respect to its neighbors and its environment.

For the sake of simplicity, we did not consider the cell deformation caused by its motion. In addition, since the cells can be seen as flat¹ and since in most of our data they do not overlap, we consider cells to be bidimensional.

We denote by Ω the domain on which cells migrate. This domain is split into two parts: the micropatterned domain Ω_π , on which cells adhere, and the domain $\Omega \setminus \Omega_\pi$, on which cells move freely. In the experiments, Ω_π is mainly composed of disjoint thin strips of polymers, but some experiments have dealt with annulus micropatterns (see Fig. 3(c)). We describe the motion and the orientation of N cells on the domain Ω .

For $0 \leq i \leq N$, the i^{th} cell at the time t is characterized by an ellipse centered at the point $\mathbf{M}_i(t)$ of the surface and whose (major axis) orientation is given by the unit vector $\mathbf{L}_i(t)$, as described in Fig. 3(a). The major and minor radii of the ellipse, respectively denoted by Λ and λ , do not depend on time: they are parameters of the model that will be fitted with the experimental data.

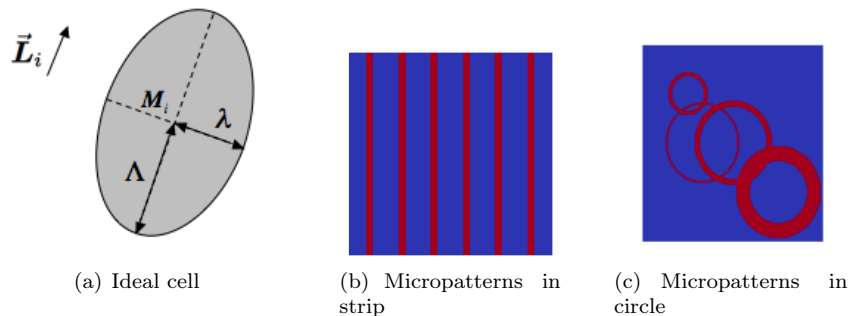


Figure 3: Schematic single cell, and examples of experimental micropatterned domain.

The heuristics of the modeling can be summarized as follows. Using the principle of the second Newton's law, which states that the net force is proportional to the acceleration, we first obtain the motion of \mathbf{M}_i , the center of the ellipsoidal cell. We then obtain the equation on \mathbf{L}_i by analogy with the orientation of a dipole subjected to a field in a bidimensional domain.

3.1 Net force acting on the cell

According to the experiments, and to the biological consideration, a single cell is subjected to the four following forces:

- A long range attractive force between the cells \mathbf{F}_c , generated by the chemical signal released by the other cells, so that cells attract themselves.

¹According to the experiments, the cells are 25 to 50 μm long, 10 to 20 μm wide and only 1 to 2 μm thick.

- A short range repulsive force \mathbf{F}_r , which prevents the overcrowding of the cells.
- A friction force \mathbf{F}_f , which describes the adhesion to the domain.
- An attractive force on the strip \mathbf{F}_a , which stacks the cell on the strip thanks to the nutrients.

The differential equation satisfied by the cell center \mathbf{M}_i reads:

$$\ddot{\mathbf{M}}_i = \mathbf{F}_c - \mathbf{F}_r - \mathbf{F}_f + \mathbf{F}_a. \quad (1)$$

Note that we have normalized cell mass to 1 in Newton's law. This is hidden in the parameters describing each force. We chose to keep the inertial term $\ddot{\mathbf{M}}_i$ because it is not clear if it can be neglected in the crowding process. The drawbacks of this choice is that small time steps have to be used, which increase the computational time. Of course one can recover the usual overdamped model by choosing carefully the coefficient of the forces which neglect the inertial term. Moreover, as our model involves the velocity of the cells in the description of the forces, it would be difficult to solve numerically the problem without taking the acceleration into account.

Let us write precisely the above forces.

3.1.1 Cell-to-cell attraction force \mathbf{F}_c

The way that endothelial cells communicate is still not clearly understood, but according to biologists (see [14]), it seems that cells produce chemoattractant that diffuse around them in order to attract their neighbors.

We denote by φ the density of chemoattractant produced by the cells on the domain Ω . For each cell, the production of φ is generated by a Gaussian Ψ supported by the cell, whose maximum is at the cell center. We assume that the diffusion of φ occurs on a smaller timescale than the cell movement. Therefore φ satisfies the Poisson equation:

$$\Delta\varphi = f_c(\mathbf{x}) \sum_{i=1}^N \Psi(\mathbf{x} - \mathbf{M}_i(t, \mathbf{x})), \quad \forall(t, \mathbf{x}) \in (0, \infty) \times \Omega. \quad (2)$$

with homogenous Dirichlet boundary conditions.

Here above the function f_c is related to the rate of production of the chemoattractant. We assume that cells produce more chemoattractant on the strip than outside, therefore f_c is the following piecewise constant function:

$$f_c(\mathbf{x}) = \begin{cases} 1 & \text{if } \mathbf{x} \in \Omega \setminus \Omega_\pi \\ \gamma_c & \text{if } \mathbf{x} \in \Omega_\pi \end{cases}, \quad \text{with } \gamma_c > 1. \quad (3)$$

This corresponds to the fact that cells that are in good condition of adhesion tends to attract the other cells more than the cell whose adhesion is weak.

The attraction force \mathbf{F}_c is then derived from φ :

$$\mathbf{F}_c(t, \mathbf{x}) = \nabla\varphi(t, \mathbf{x}), \quad \forall(t, \mathbf{x}) \in (0, +\infty) \times \Omega.$$

From the numerical point of view, φ (and thus the attraction force \mathbf{F}_c) is computed on the cartesian grid, while the cells move freely in the domain. Therefore, the value of \mathbf{F}_c is projected on each endothelial cell $(\mathbf{M}_j)_{j=1}^N$, using the projection method described by Min and Gibou [19].

3.1.2 Repulsive force

It has been experimentally observed that two cells do not overlap. This fact is taken into account by a repulsive term which prevents the cell overcrowding:

$$\mathbf{R}(\mathbf{M}_i) = \sum_{\substack{j=1 \\ j \neq i}}^N \frac{\mathbf{M}_i - \mathbf{M}_j}{\|\mathbf{M}_i - \mathbf{M}_j\|^3}. \quad (4)$$

The power 3 ensures that the repulsive force is an inverse-square law: it is inversely proportional to the square of the distance between 2 cells. We chose such an inverse square law so that repulsion force is bigger than the attraction force. Actually in 2 dimensions the Green function of the Laplacian is $\log(r)$ and therefore the attraction force is of order $1/r$: to prevent the overlapping, we have to impose a repulsion greater than the attraction for short distances.

Since the cells are ellipsoidal, it is necessary to add a multiplication factor in front of \mathbf{R} . Actually suppose that two cells are located at the points \mathbf{M}_i and \mathbf{M}_j (see Fig 4). When cells are aligned along $\overrightarrow{\mathbf{M}_i \mathbf{M}_j}^\perp$ (see Fig.4(a)), the repulsion force is the lowest since the distance between the cell boundaries is the greatest. On the contrary, in the configuration of Figure 4(b) the cell alignment is parallel to $\overrightarrow{\mathbf{M}_i \mathbf{M}_j}$, the repulsion force reach its maximum value. We therefore

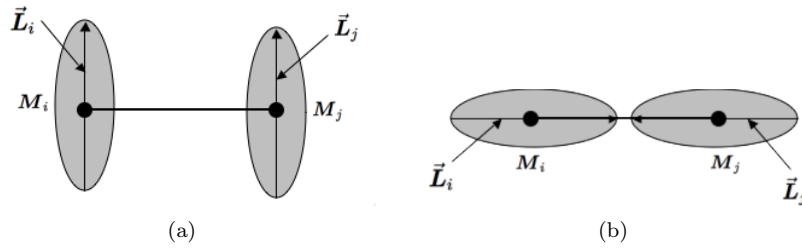


Figure 4: Influence of the cell orientation on the cell-cell distance.

introduce the factor $\beta(\mathbf{L}_i)$, which depends on the orientation of the i^{th} cell:

$$\beta(\mathbf{L}_i) = \frac{\Lambda - \lambda}{\lambda} \left(\sum_{\substack{j=1 \\ j \neq i}}^N \left(\left| \frac{\mathbf{M}_i - \mathbf{M}_j}{\|\mathbf{M}_i - \mathbf{M}_j\|} \cdot \mathbf{L}_i \right| + \left| \frac{\mathbf{M}_i - \mathbf{M}_j}{\|\mathbf{M}_i - \mathbf{M}_j\|} \cdot \mathbf{L}_j \right| \right) \right) + 1. \quad (5)$$

The coefficient $(\Lambda - \lambda)/\lambda$ is introduced in order to take the cell shape into account: for rounded cell it vanishes since there is no cell orientation, and the more elongated the cell, the greater it is. The repulsive force now writes

$$\mathbf{F}_r(\mathbf{L}_i, \mathbf{M}_i) = \gamma_r \beta(\mathbf{L}_i) \mathbf{R}(\mathbf{M}_i), \quad (6)$$

where γ_r is a parameter fitted with the experiments.

3.1.3 Friction force

The friction force is proportional to the cell velocity, it thus reads

$$\mathbf{F}_f(\mathbf{M}_i) = \alpha_f f_f(\mathbf{M}_i) \dot{\mathbf{M}}_i,$$

where the friction coefficient f_f describes the adherence of the domain. Since cells move slowly on the strip, $f_f(\mathbf{M}_i)$ is a piecewise constant function given by :

$$f_f(\mathbf{M}_i) = \begin{cases} 1 & \text{if } \mathbf{M}_i \in \Omega \setminus \Omega_\pi \\ \gamma_f & \text{if } \mathbf{M}_i \in \Omega_\pi \end{cases}, \quad \text{with } \gamma_f > 1. \quad (7)$$

3.1.4 Attractive force of the adhesive areas

If a part of a cell is located on the micropatterned polymer region, it will find nutrients and oxygens on the active principle that will attract the whole cell on the strip. On the contrary, if the cell is completely on the polymer region, or outside this region, the attraction force \mathbf{F}_a due to the strip vanishes.

We use the above function f_f , which describes the adherence of the domain, to determine whether the cell is straddling the polymer region and the outer domain. Actually, since the distance between two strips is larger than the cell size, the term

$$f_f(\mathbf{M}_i + \Lambda \mathbf{L}_i) - f_f(\mathbf{M}_i - \Lambda \mathbf{L}_i)$$

vanishes if the point $\mathbf{M}_i + \Lambda \mathbf{L}_i$ and $\mathbf{M}_i - \Lambda \mathbf{L}_i$ are on the same domain. It is positive and equal to $\gamma_f - 1$ if $\mathbf{M}_i + \Lambda \mathbf{L}_i$ is on the strip and not $\mathbf{M}_i - \Lambda \mathbf{L}_i$, and thus the cell will tend to move in the direction of \mathbf{L}_i . On the other hand, if $\mathbf{M}_i - \Lambda \mathbf{L}_i$ is on the strip and not $\mathbf{M}_i + \Lambda \mathbf{L}_i$, then it equals $1 - \gamma_f$, and the cell will tend to move in the direction of $-\mathbf{L}_i$. Similar considerations by replacing Λ by λ and \mathbf{L}_i by \mathbf{L}_i^\perp ensures that \mathbf{F}_a is thus given by

$$\begin{aligned} \mathbf{F}_a(\mathbf{M}_i, \mathbf{L}_i) = & \gamma_a (f_f(\mathbf{M}_i + \Lambda \mathbf{L}_i) - f_f(\mathbf{M}_i - \Lambda \mathbf{L}_i)) \mathbf{L}_i \\ & + \gamma_a (f_f(\mathbf{M}_i + \lambda \mathbf{L}_i^\perp) - f_f(\mathbf{M}_i - \lambda \mathbf{L}_i^\perp)) \mathbf{L}_i^\perp, \end{aligned} \quad (8)$$

where γ_a is a numerical parameter.

3.2 Orientation of the cells

As mentioned before, the deformation of endothelial cells is a very complex process, which is not taken into account in our simple model. Nevertheless, the cell alignment plays an important role in the tube-like formation. We therefore have chosen to take this alignment behavior into account by modeling the orientation \mathbf{L}_i of each cell.

3.2.1 Heuristics of cell alignment

Before stating the equation satisfied by \mathbf{L}_i , we introduce the ‘‘alignment’’ vector field Φ defined from $\mathbb{R}^2 \times \mathbb{R}^2$ onto \mathbb{R}^2 by

$$\begin{aligned} \Phi : \quad & \mathbb{R}^2 \times \mathbb{R}^2 \rightarrow \mathbb{R}^2 \\ & (\mathbf{U}, \mathbf{V}) \mapsto (\mathbf{U} \cdot \mathbf{V})(\mathbf{U} \cdot \mathbf{V}^\perp) \mathbf{U}^\perp \end{aligned} \quad (9)$$

In order to understand the above vector field Φ , suppose that \mathbf{V} is a given vector of \mathbb{R}^2 . Let \mathbf{U} be a time-dependent vector of \mathbb{R}^2 and let θ be the angle between \mathbf{U} and \mathbf{V} in the left-handed orientation. The orientation of \mathbf{U} along \mathbf{V} is easily written by the following ordinary differential equation on θ :

$$\dot{\theta} = -\frac{1}{2} \sin(2\theta),$$

such that $\{0, \pi\}$ are stable equilibrium points while $\{-\pi/2, \pi/2\}$ are unstable. This differential equation can be written in terms of \mathbf{U} thanks to Φ :

$$\dot{\mathbf{U}} = \Phi(\mathbf{U}, \mathbf{V}).$$

3.2.2 Differential equation for L_i

According to the experiments, the cell orientation is driven by three phenomena:

- Alignment along the cell velocity.
- Alignment along the orientation of their neighbors.
- Alignment along the local tangent vector \mathbf{S}_i of the boundary of micropatterns at the closest point of M_i .

We therefore infer the differential equation for L_i :

$$\begin{aligned} \dot{L}_i = & \omega_v \Phi(L_i, \frac{\dot{M}_i}{\|\dot{M}_i\|}) + \omega_c \sum_{\substack{j=1 \\ j \neq i}}^N \frac{\Phi(L_i, L_j)}{\|M_i - M_j\|^2} \lambda^2 \\ & + \omega_\pi \beta_\pi(M_i) \Phi(L_i, \mathbf{S}_i). \end{aligned} \quad (10)$$

Here again it is natural to introduce an inverse-square law for the interaction between two cells. The above function β_π is given by

$$\begin{aligned} \beta_\pi(M_i) = & 4f_f(M_i) - f_f(M_i + \Lambda L_i) - f_f(M_i - \Lambda L_i) \\ & - f_f(M_i + \lambda L_i) - f_f(M_i - \lambda L_i), \end{aligned} \quad (11)$$

it ensures that if the cell is entirely on (or out of) the micropatterns, the cell does not try to align but if the cell is partly on the strip then it tends to align along the direction of the strip. Here above, the parameters ω_v , ω_c and ω_π are homogeneous to the inverse of the characteristic time of each alignment. They will be fitted with the experiments.

4 Simulations and experiments

In order to study the consistency of our model, we compare the simulation with the experimental results. We focus on experimental results described in [15]. The domain Ω is a square of 1mm^2 , on which 500 cells are randomly distributed, in accordance with the experiments. To compute the distribution of the chemoattractant φ given by (2), the domain Ω is meshed thanks to a cartesian grid of 100×100 elements. Three different widths of the adhesive areas are considered: 10, 50 and 100 μm , with the same spacing of 100 μm between the strips.

We emphasize that in order to validate the model we first optimized the parameters for one specific experiment: here we present the case of strips of 100 μm width, and then, taking the values of the parameters for this specific experiment and changing the geometry, we compare the numerical results to the experimental data.

4.1 Numerical method

The discretization of the time derivatives are made using a "leap-frog" scheme for the acceleration and a centered scheme for the velocity. Initially, cells are randomly distributed on the domain Ω .

The Laplace problem (2) is discretized using a centered finite volume scheme (cf [7]). The variables are computed at the center of each element of the mesh. The homogenous Neumann condition is imposed using a penalty method. This allows us to define a general framework to deal with different kinds of geometries (cf Fig. 3(b) and Fig. 3(c)). We use a solver implemented on the academic library eLYSe.

4.2 Calibration of the model

4.2.1 Cell shape

In [15], for all three cases, the authors give the cell shapes distribution at the end of the experiments. They measured an approximation of the circularity \mathcal{C} (cf Fig 5(a)) of the cells corresponding to the rapport of the major axis with the minor axis. They also give the area of the cells \mathcal{A} on the three different geometries (cf Fig. 5(b)).

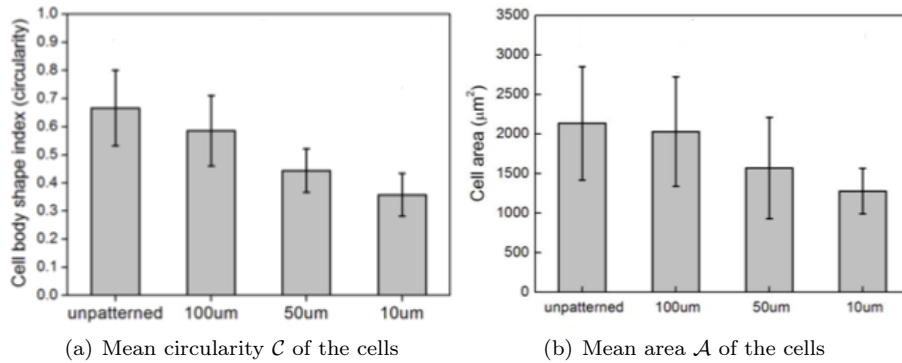


Figure 5: Cells shape informations measured at the end of the experiment. [15]

These measures determine entirely the cell shape parameter of the model thanks to the relations:

$$\mathcal{C} = \lambda/\Lambda, \quad \mathcal{A} = \pi\Lambda\lambda.$$

Therefore, for each test-case the value of Λ and λ are given by table 1. Since our phenomenological

Strip width	10 μm	50 μm	100 μm
Λ : Semi major axis (μm)	59.6	59.7	59.2
λ : Semi minor axis (μm)	21.4	26.2	34.3

Table 1: Major and minor axes of the cells with respect to the width of the strips.

model does not come from physical consideration, the parameters involved in the modeling cannot be measured. Therefore it is essential to fit the parameters with the experiments.

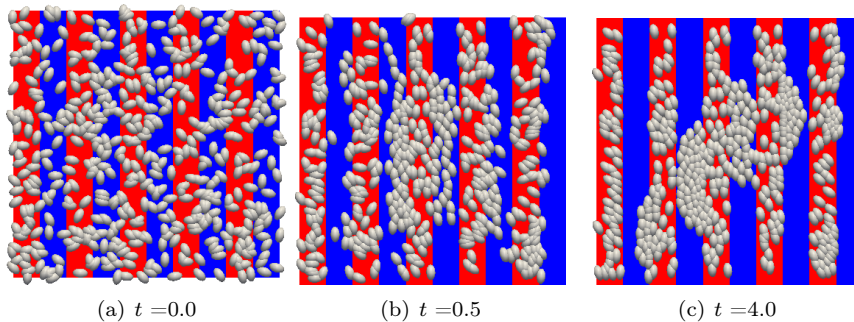


Figure 6: Position and orientation of endothelial cells on 100 μm strips at different times.

We first consider the experiments with strips of 100 μm width. We then chose the parameters given by table 2 to fit with the experiments. In the next paragraph, the consistency of the model

γ_c	γ_r	γ_f	α_f	γ_a	ω_v	ω_c	ω_π
10	10^{-5}	120	10	0.05	1	0.2	0.2

Table 2: Parameters set to fit with the experiments of 100 μm .

will be shown in the next section by comparing the numerical results with the experiments. We keep the parameters of table 2 and we change the width of the strips as well as the final shape of the cells in accordance with the experiments.

A trickier question would be to solve an inverse problem and to find all the set of parameter that lead to an adequate fit of the data. Note that this is a difficult problem which we will not address in this paper. The above set of parameter fit with all the considered test cases.

4.3 Qualitative results on the cell motility towards the micropatterns

We first provide qualitative results of the cell migration for strips of 100 μm width. In Fig.6, the positions of the endothelial cells at different times are given. The adhesive areas are colored in red, the outer domain in blue and the cells are plotted as white ellipses. In accordance with the experiments, we observe that the cells migrate towards the strips. Note that, as for the experiments, some cells remains out of the strips since they do not have enough space on the adhesive areas.

In the experiments the cells are washed out before counting. Numerically speaking, this corresponds to take out the cells that are not on the strips. Thus in Fig. 7, we present the final cell position on the strip only, at the end of the simulation (*i.e.* when the cells are almost completely stabilized).

The results are qualitatively in agreement with the experiments.

4.4 Quantitative results on cell alignment

We now focus on the orientation of the cells in the three previous configurations. In [15], at the end of the experiment, the authors measure the angle θ (in degree) between the major axis of a cell with the axis of the adhesive areas as shown in the Fig. 8. For each configuration, six experiments are performed and histograms of the mean values are obtained. This is consistent

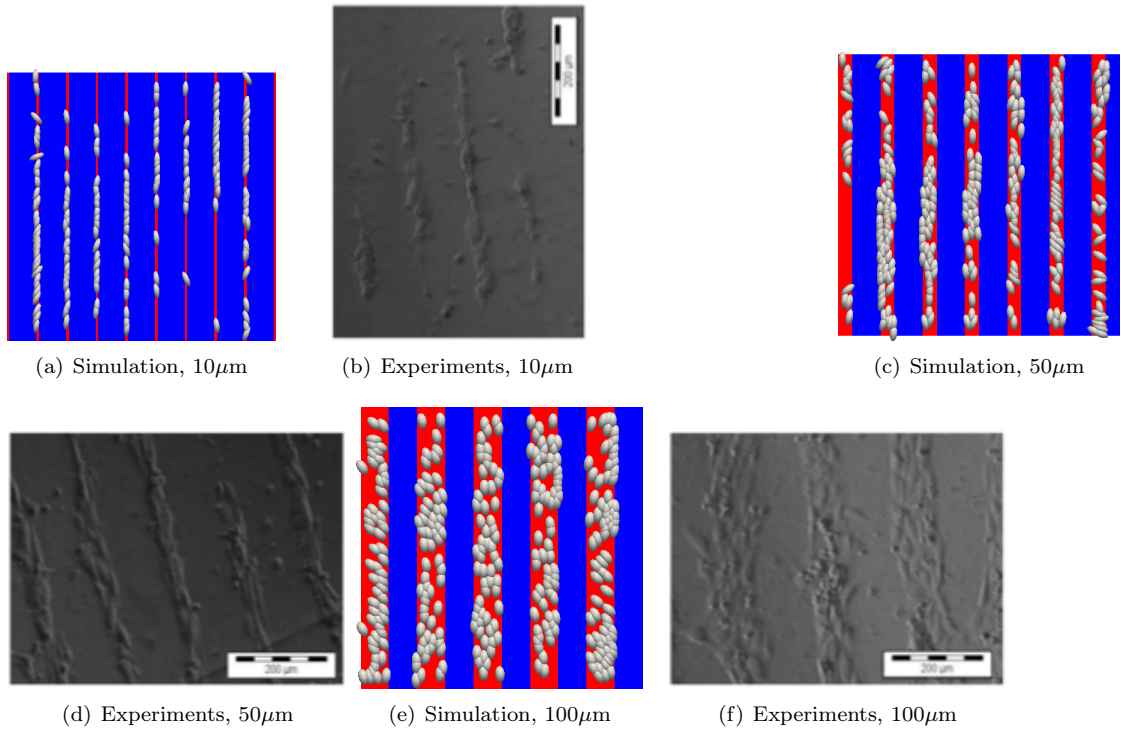


Figure 7: Comparison between experimental results of [15] and numerical simulations

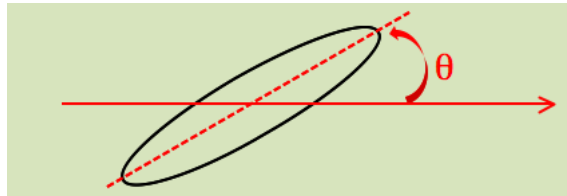


Figure 8: Definition of the angle θ for a cell.

with the number of experiments performed for each configurations ([14]). When θ is less than 10° , we have considered that the cells are aligned with the strip.

We first consider the $100 \mu\text{m}$ width strips case. We have computed the angle θ of the adhered cells for different initial conditions. We present experimental and numerical results in Fig. 9. The results are qualitatively and quantitatively in accordance with the experiments. Experimentally, 27% of the cells are considered to be aligned, numerically, this value is equal to 33.78%. Moreover, the mean value of the cell body alignment angle is equal to 25.9 in [15] and we obtain a closed value: 23.10. (see also Tables 3–4).

For the domain composed by $10 \mu\text{m}$ width strips, the results are also in accordance with the experiments, as shown in Fig. 10.

Note that the number of aligned cells is more important on thin strips. Numerically, 70.54 % of the cells have an angle belonging between 0° and 10° whereas experimentally one obtains

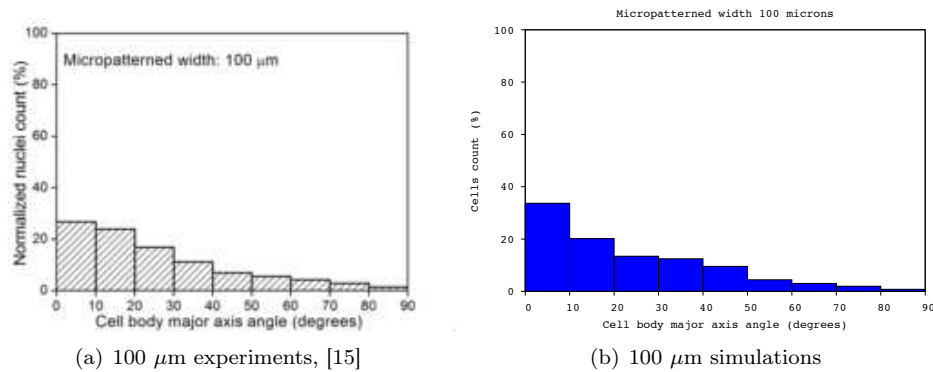


Figure 9: Cell alignment on 100 μm strips, comparison between experimental (a) and numerical (b) results.

73 % of the cells. The mean alignment angle value obtained numerically is equal to 8.8° and experimentally it is equal to 9.98° .

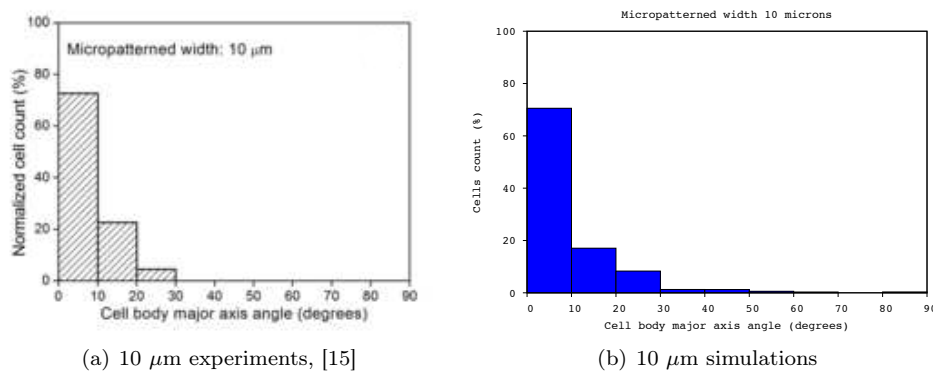


Figure 10: Cell alignment on 10 μm strips in the experiments Fig. 10(a) and in the simulation Fig.10(b).

Let us now take 50 μm width strips. As previously, we show, in Fig. 11, the cell alignment at the end of the experiment.

The distribution of the angle have qualitatively the expected behavior, the cells are more aligned than in the case of 10 μm strips. One observes that 42% of the cells are aligned, when we have obtained 47.19%. We obtain an angle mean value of 14.62° , which is very closed to the experimental measurements: 15.2° .

4.5 Sensitivity analysis

We are interested here in studying the influence of the parameter involved on the orientation of the cells: ω_v , ω_c , and ω_π on two different results: the mean angle value and the percentage of aligned cells. We use Morris's method introduced in [20]. We let one parameter vary and compute the elementary variation of the results for sample points of the parameter space. This

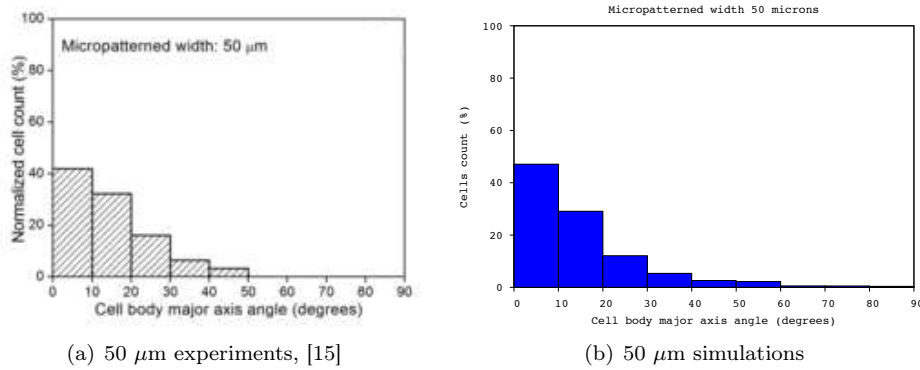


Figure 11: Cell alignment on $50\mu\text{m}$ strips, comparison between experimental (a) and numerical (b) results.

give rise to a random variable. We then compute the mean m and the standard deviation S of this random variable and the corresponding points are plotted in a plan (m,S) . The results obtained are presented in Fig 12. We observe that the mean value and the standard deviation obtained for ω_c , and ω_π are important meanwhile they are low when considering the influence of ω_v . The mean angle value and the percentage of aligned cells is strongly influenced by the intensity of the alignment along the strips and along the orientation of the neighbors.

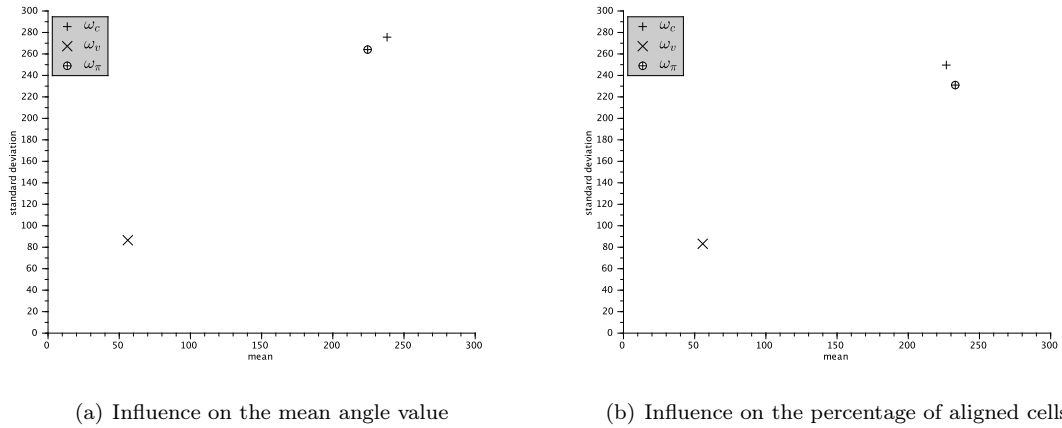


Figure 12: Sensitivity analysis of the ω_v (orientation along the velocity field), ω_c (orientation along the neighbors of the cells), and ω_π (orientation along the strips) parameters .

5 Conclusion

We have provided a simple agent-based model that describes the cell motility on bioactive micropatterned polymers thanks to classical mechanics consideration. The model has been derived by analogy to the Newton laws: the acceleration of the cell is driven by four forces, which describe

the cell-cell interactions and the influence of the domain on the cell motility. We also describe the orientation of the cell, similarly to a dipole subjected to a force field. This model involves phenomenological parameters whose values have been estimated to fit the experiments. Changing the configuration of the strips, but keeping the same parameters, we obtain results that are quantitatively in accordance with the experiments. The comparison between the experimental measurement of the cell orientation to the simulation are summarized in tables 3–4. As mentioned above, the numerical results are qualitatively in good agreement with the experimental data.

	Percentage of aligned cells along the strips		
	10 μm	50 μm	100 μm
Exp. Data	73	42	27
Num. Res.	70.54	47.1	33.68

Table 3: Angle of the mean cell alignment along the patch

	Angle of the mean alignment along the strips		
	10 μm	50 μm	100 μm
Exp. Data	$8.6 \pm 6.1^\circ$	$15.2 \pm 9.6^\circ$	$25.9 \pm 15.8^\circ$
Num. Res.	9.98°	14.62°	23.10°

Table 4: Cell alignment of the experiments (Exp. Data.) given by [15] compared with the numerical simulations (Num. Res.)

According to both experimental and numerical results (Fig. 10 11 and 9) the cell alignment is more efficient on thin strips than on larger ones.

Moreover, the forces that we have used are enough to describe both adhesion and orientation of the cells. This may be seen, in some sense, as a basic framework for the description of cell motion on scaffold.

References

- [1] K. Anselme, P. Davidson, A.M. Popa, M. Liley, and L. Ploux. The interaction of cells and bacteria with surfaces structured at the nanometre scale. *Acta Biomaterialia*, 6:3824–3846, 2010.
- [2] M. Bagnat and K. Simons. Cell surface polarization during yeast mating. *Proceedings of the National Academy of Sciences*, 99(22):14183–14188, 2002.
- [3] C.S. Chen, M. Mrksich, S. Huang, G.M. Whitesides, and D.E. Ingber. Geometric control of cell life and death. *Science*, 276(5317):1425–1428, 1997.
- [4] T. Colin, M.-C. Durrieu, J. Joie, Y. Lei, Y. Mammeri, C. Pognard, and O. Saut. Modeling of the migration of endothelial cells on bioactive micropatterned polymers. *Mathematical biosciences and engineering*, to appear, 2012.
- [5] L.E. Dike, C.S. Chen, J. Tien, G.M. Whitesides, and D.E. Ingber. Geometric control of switching between growth, apoptosis, and differentiation during angiogenesis using micropatterned substrates. *In Vitro Cell. Dev. Biol.*, 35:441–448, 1999.

- [6] D. Drasdo, S. Dormann, S. Hoehme, and A. Deutsch. Cell-based models of avascular tumor growth. In *Function and Regulation of Cellular Systems*, Mathematics and Biosciences in Interaction, pages 367–378. Birkhäuser Basel, 2004.
- [7] R. Eymard, T. Gallouet, and R. Herbin. *Finite Volume Methods*. Handbook of Numerical Analysis., 2007.
- [8] A. Folch and M. Toner. Microengineering of cellular interactions. *Annu. Rev. Biomed. Eng.*, 2:227–256, 2000.
- [9] R. J. Hawkins, O. Bénichou, M. Piel, and R. Voituriez. Rebuilding cytoskeleton roads: Active-transport-induced polarization of cells. *Physical Review E*, 80, 2009.
- [10] J. Irazoqui, A. Gladfelter, and D. Lew. Scaffold-mediated symmetry breaking by cdc42p. *Nat. Cell Biol.*, 5(12):1062–1070, 2003.
- [11] Y. Ito. Surface micropatterning to regulate cell functions. *Biomaterials*, 20(23/24):2333–2342, 1999.
- [12] R.K. Jain, P. Au, J. Tam, D.G. Duda, and D. Fukumura. Engineering vascularized tissue. *Nat. Biotechnol.*, 23:821–823, 2005.
- [13] M. Kamei, W.B. Saunders, K.J. Bayless, L. Dye, G.E. Davis, and B.M. Weinstein. Endothelial tubes assemble from intracellular vacuoles in vivo. *Nature*, 442:453–456, 2006.
- [14] Y. Lei. *Biochemical and microscale modification of polymer for endothelial cell angiogenesis*. PhD thesis, Université Bordeaux 1, 2012.
- [15] Y. Lei, O.F. Zouani, L. Rami, C. Chanseau, and M.-C. Durrieu. Modulation of lumen formation by microgeometrical bioactive cues and migration mode of actin machinery. *Small*, doi:10.1002/sml.201202410, 2012.
- [16] Y. Lei, O.F. Zouani, M. Rémy, C. Ayela, and M.-C. Durrieu. Geometrical microfeature cues for directing tubulogenesis of endothelial cells. *PLoS ONE*, 7(7):e41163, 2012.
- [17] B. Lubarsky and M.A. Krasnow. Tube morphogenesis: making and shaping biological tubes. *Cell*, 112:19–28, 2006.
- [18] K. Madden and M. Snyder. Cell polarity and morphogenesis in budding yeast. *Annual Reviews in Microbiology*, 52(1):687–744, 1998.
- [19] C. Min and F. Gibou. A second order accurate level set method on non-graded adaptive cartesian grids. *Journal of Computational Physics*, 225:300–321, 1997.
- [20] M.D. Morris. Factorial sampling plans for preliminary computational experiments. *Technometrics*, 33(2):161–174, 1991.
- [21] R.M. Nerem. Tissue engineering: the hope, the hype, and the future. *Tissue Eng.*, 12(1143-1150), 2006.
- [22] D.V. Nicolau, Taguchi T., H. Taniguchi, H. Tanigawa, and S. Yoshikawa. Patterning neuronal and glia cells on light-assisted functionalized photoresists. *Biosens. Bioelectron.*, 14(3):317–324, 1999.
- [23] E.A. Phelps and A.J. Garcia. Engineering more than a cell: vascularization strategies in tissue engineering. *Curr. Opin. Biotechnol.*, 21:704–709, 2010.

- [24] T.-H. Tsai. Simulations of endothelial cells clusters migration in angiogenesis. *The SIJ Transactions on Computer Science Engineering & its Applications (CSEA)*, 1(4):111–115, 2013.
- [25] R. Wedlich-Soldner, S. Altschuler, L. Wu, and R. Li. Spontaneous cell polarization through actomyosin-based delivery of the cdc42 gtpase. *Science*, 299(5610):1231–1235, 2003.
- [26] R. Wedlich-Soldner, S.C. Wai, T. Schmidt, and Rong Li. Robust cell polarity is a dynamic state established by coupling transport and gtpase signaling. *The Journal of Cell Biology*, 166(6):889–900, 2004.



**RESEARCH CENTRE
BORDEAUX – SUD-OUEST**

351, Cours de la Libération
Bâtiment A 29
33405 Talence Cedex

Publisher
Inria
Domaine de Voluceau - Rocquencourt
BP 105 - 78153 Le Chesnay Cedex
inria.fr

ISSN 0249-6399